Contents lists available at ScienceDirect

Arabian Journal of Chemistry

journal homepage: www.ksu.edu.sa

BZT substitution effect on the characteristics of (1-x) MT – x BZT composite ceramics synthesized by the sol–gel method

Mahjoub DAOUDY *, Najwa GOUITAA, Fatima Zahra AHJYAJE, Taj dine LAMCHARFI, Farid ABDI

Signals, Systems and Components Laboratory (LSSC), Electrical Engineering Department, University Sidi Mohamed Ben Abdellah USMBA, FST. Fez, Imouzzer Road B.P. 2202, Morocco

A R T I C L E I N F O

Keywords:
Ceramic
BZT-MT
Sol–gel
X-ray diffraction
Dielectric properties
Phase transition

A B S T R A C T

This paper addresses a crucial gap in the effect of adding $BaZr_{0.1}Ti_{0.9}O_3$ (BZT) on the structural, microstructural, dielectric, and electrical properties of $MgTiO_3$ (MT) material. These ceramics with the chemical composition (1-x) MT – x BZT were synthesized with different compositions ranging from × = 0.0 to 1.0 with a 0.1 step using the sol–gel reaction process. The X-ray diffraction (XRD) results and Rietveld refinement analysis showed the formation of a tetragonal phase with the P4mm space group for the BZT sample and a hexagonal phase with the R-3 space group for MT ceramics, without any secondary phases. However, (1-x) MT – x BZT composites with × ranging from × = 0.1 to 0.9, showed a coexistence of tetragonal (P4mm) and hexagonal (R-3) phases. Scanning Electron Microscopy (SEM) was used to investigate the morphology and grain size of the compounds. The SEM results revealed a clear decrease in grain growth for x = 0.6 of BZT content with the higher density. Furthermore, the dielectric properties of these composites were studied by impedance spectroscopy, which showed a single diffuse dielectric phase transition for all the BZT-MT composites. There was a clear increase in dielectric permittivity (ε_r') value with the increase of the BZT content. This broad phase transition is highly desired and has not been observed in previous studies. The obtained composite ceramics could open the way to lead new applications in microelectronic devices.

1. Introduction

In recent years, a lot of interest has been focused on the development of lead-free perovskites due to their excellent dielectric, electrical proprieties, and environmental friendliness (Mondal et al., 2018). Barium titanate $BaTiO_3$ (BT) ceramic is the first lead-free metal oxide material with ferroelectric behavior (Zheng et al., 2023; Chen, 2020). Serval years after its invention, BT has become one of the most important base materials for dielectric ceramics due to its excellent dielectric proprieties, such as a high dielectric constant with a high curie temperature (T_c), low dielectric loss, and environmental friendliness (Gouitaa et al., 2018; Yang et al., 2021). These proprieties make BT the perfect candidate for many technological and industrial applications, like dynamic memories, capacitors, sensors, microwave tunable devices, and so on (Amu-Darko et al., 2022; Baryshnikov et al., 2015).

The BT has a perovskite structure ABO_3, in which the A-site is filled with an alkaline metal ion (Ba^{+2}), and the B-site is represented by a transition metal ion (Ti^{4+}) (Hu et al., 2020). The BT structure possesses an octahedrally organized small metal cation in tightly packed layers on the B-site and a large metal cation with oxygen ions placed closely together in layers on the A-site (Fahad et al., 2022; Yang et al., 2021).

In its pure form, BT is an electrically insulating material, but it becomes semi-conducting by inserting dopants. These dopants affect and/or enhance the material structure, dielectric proprieties, polarization process, and transition temperature (Gouitaa et al., 2018; Dai, 2020; Zhou et al., 2019). Similarly, BT exhibits improved properties as a result of foreign ions being doped at the Ba-site and/or Ti-site at suitable dopant concentrations to generate a material widely used in a variety of applications (Fahad et al., 2022; Shukla et al., 2019; Yang et al., 2020).

Recently, several works have investigated the substitution of BT by zirconium (Zr) as a dopant at the Ti-site to form barium zirconate titanate $BaZr_xTi_{1-x}O_3$ (BZ_xT) (Elbasset et al., 2015; Sateesh et al., 2015),

Peer review under responsibility of King Saud University.

* Corresponding author.
E-mail address: mahjoub.daoudy@usmba.ac.ma (M. DAOUDY).

https://doi.org/10.1016/j.arabjc.2023.105392
Received 22 July 2023; Accepted 24 October 2023
Available online 27 October 2023

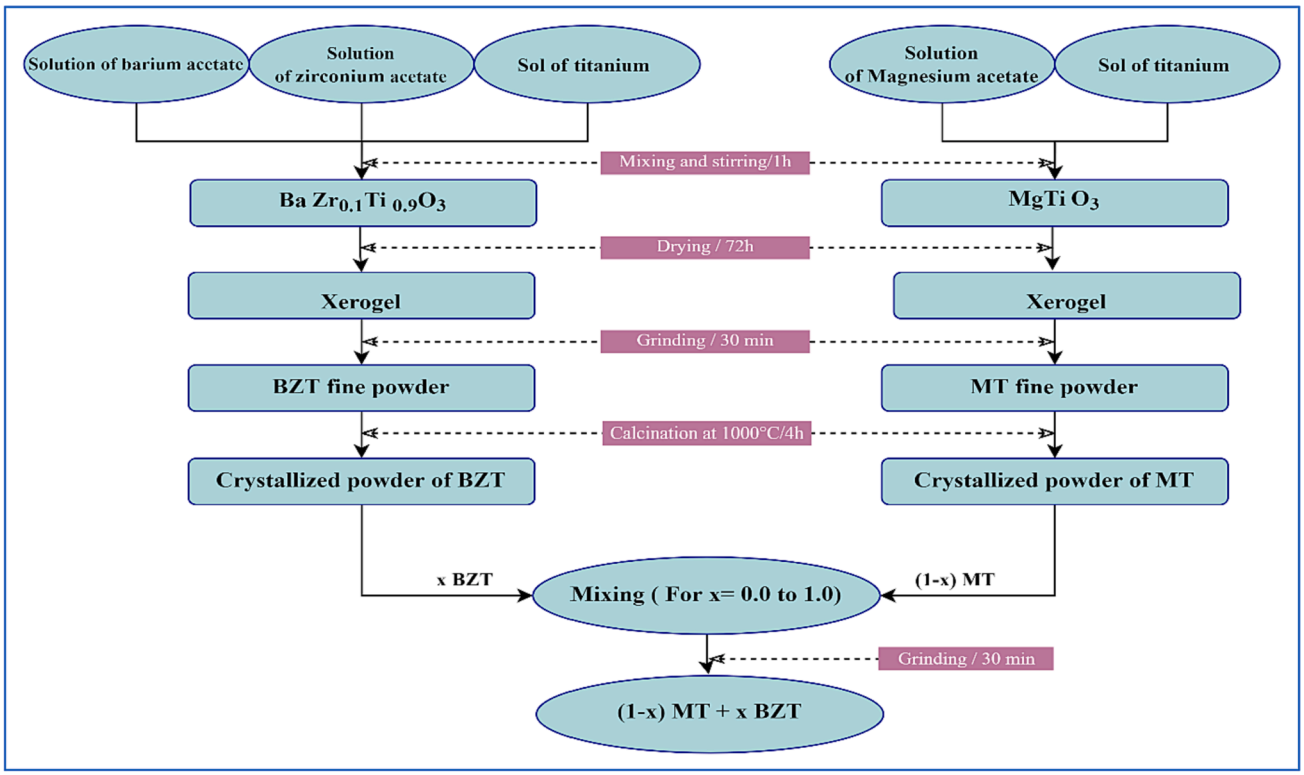

Fig. 1. Flow chart of the sol–gel elaboration of (1-x) MT – x BZT composites ceramics.

where × represents the Zr concentration. The Zr^{4+} ionic radius (0.087 nm) is greater than that of Ti^{4+} (0.0685 nm), which can improve the chemical stability of the BZ_xT materials, enhancing their dielectric proprieties and reducing the transition temperature. The characteristics of BZ_xT make them more appropriate for different applications, such as ceramic capacitors, sensors, solar cells, piezoelectric actuators, and tunable microwave devices like phase shifters and filters (Binhayeeniyi et al., 2010). A study by A. Elbasset et *al.* investigated the impact of Zr content in BZ_xT material (x = 0 –15 at % with a step of 2.5 %). They found that at x = 10 %, the material exhibited the best proprieties such as an increase in the dielectric constant, a reduce in the dielectric loss, and a lower curie temperature (Elbasset et al., 2015). In this study, we chose to work with a Zr concentration of 10 % because of its dielectric constant ($\varepsilon_r \sim 2830$), dielectric loss ($\delta \sim 0.012$), good thermal stability, and tetragonal perovskite structure with P4mm space group (a = b = 4.0269 Å, c = 4.0319 Å) at ambient temperature as reported in previous studies (Jamil et al., 2015).

On the other hand, Magnesium Titanate $MgTiO_3$ (MT) ceramic is still the most important material widely studied and used in microwave frequencies (Jo et al., 2015; Kumar et al., 2012). It exhibits an exceptionally low dielectric loss (10^{-4}) and intermediate dielectric constant ($\varepsilon_r \sim 17$) (Ni et al., 2021), making it an appropriate candidate for various microwave applications such as antennas, dielectric resonators, capacitors, and filters (Xu, 2018; Wang and Yan, 2021). However, the researches revealed that MT ceramic has a hexagonal structure with an R-3 space group (a = b = 5.441 Å and c = 13.644 Å) (Li et al., 2022; Ni et al., 2021).

In 2008, L.N. Gao et *al.* prepared hetero-structured thin films of $BaZr_{0.2}Ti_{0.8}O_3$ – $MgTiO_3$ using the sol–gel technique with a concentration of Zr equal to 20 %. They found that the sample has a perovskite and polycrystalline structure and MT has a significant impact on reducing the grain size (Gao et al., 2008). Subsequently, R. Pengrong et *al.* studied (1-x) $BaZr_{0.25}Ti_{0.75}O_3$ – x MgO (x = 0.1, 0.2, 0.3, 0.4) composite ceramics with 25 % of Zr content prepared by solid-state route, demonstrated that it exists only BZT and MgO phases, with no other phases present at room temperature. They also revealed that adding MgO significantly decrease the dielectric permittivity and the dielectric loss (Ren et al., 2011). Moreover, by employing a similar solid-state method, Yuan Xu et *al.* also reported the effect of MgO addition on the proprieties of $BaZr_{0.15}Ti_{0.85}O_3$ ceramic with 15 % of Zr content according to $BaZr_{0.25}Ti_{0.75}O_3$ – x mol % MgO (x = 0.0, 0.25, 0.50, 1.0, 1.5). The findings indicate that the addition of MgO into the BZT ceramic, give a decrease in the dielectric constant, reduce in the dielectric loss, and gradually reduced in the average grain size (Xu, 2019).

The present study focuses on the elaboration of (1-x) MT – x BZT (where x = 0.0 to 1.0) composite ceramics by the sol–gel route, and evaluating the impact of BZT (10 % of Zr content) on the structural, microstructural, dielectric, and electrical proprieties of MT ceramic through various characterization methods such as DRX, SEM, Fourier-transform infrared spectroscopy (FT-IR), dielectric and electrical measurements.

2. Experimental

The solid solution (1-x) MT – x BZT ceramics were synthesized via the sol–gel reaction, with a composition range from x = 0.0 to 1.0 with a 0.1 step. The different steps related to the preparation of the composites are schematized in the flow chart shown in Fig. 1.

In the first stage, BZT powder was prepared using barium acetate trihydrate (Ba $(CH_3COO)_2$, $3H_2O$), zirconium acetate (Zr $(CH3COO)_4$, xH_2O), and sol of titanium, which were dissolved in distilled water as solvent. The obtained solutions were blended in stoichiometric quantities following to the chemical formula $BaZr_{0.1}Ti_{0.9}O_3$ (BZT) and stirred for 1 h to increase the homogeneity of the solution. Then, the solution was destabilized by drying it in the oven at 80 °C for 72 h. The resulting powder was ground in an agate mortar and calcined at 1000 °C/4 h using a programmable oven to form the desired powder. In the second stage, MT powder was elaborated using Magnesium acetate (Mg $(CH_3COO)_4$, xH_2O) and a titanium sol as initial precursors, then followed the same procedure as the BZT powder synthesis. The formed MT

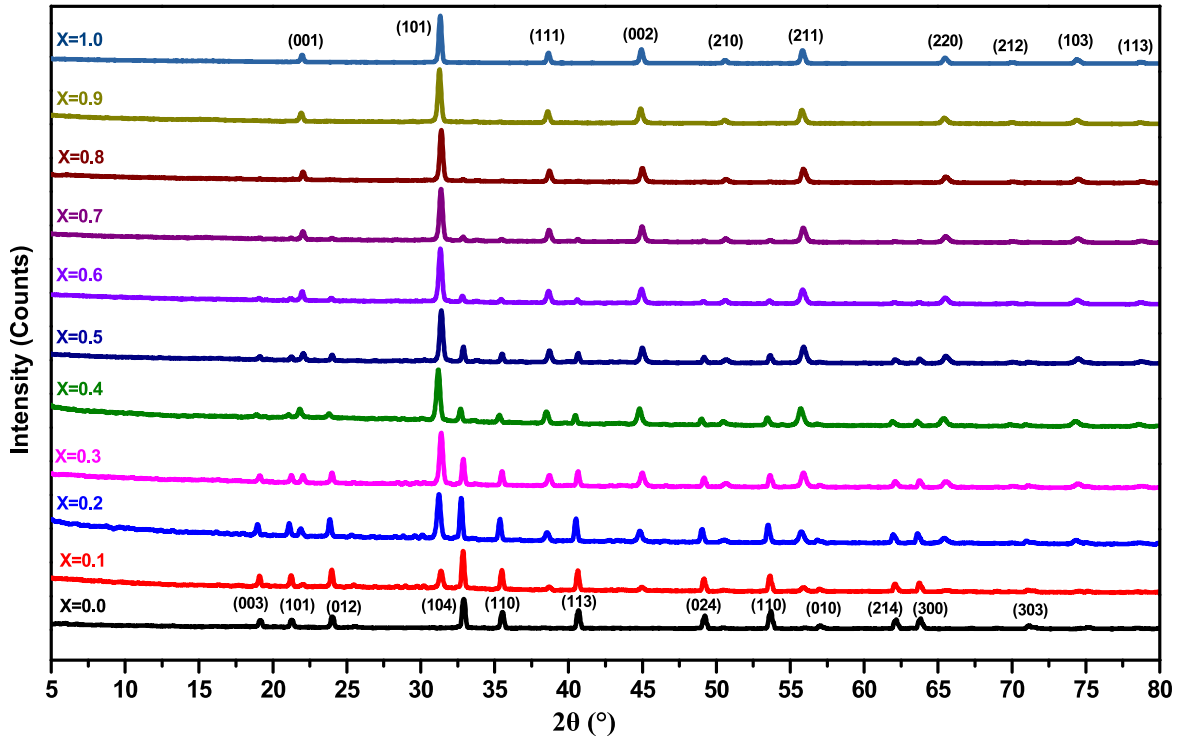

Fig. 2. X-ray diffraction diagrams of (1-x) MT – x BZT samples for × = 0.0 to 1.0.

powder was calcined at 1000 °C/4h.

The last step involved mixing and grinding the two calcined BZT and MT powders for 30 min in stoichiometric quantities in molar percent to form a composite according to the formula (1-x) MT – x BZT, where × ranged from 0.0 to 1.0. The formed composite powders were pressed into cylindrical pellets form of about 12 mm in diameter and 1 mm in thickness under a uniaxial pressure of 8 tons. These pellets were finally sintered at 1100 °C/6h using a programmable oven with a heating rate of 3 °C/min.

The phase formation of the obtained compounds was determined by structural characterization, such as powder XRD and FT-IR. The surface morphology and grain sizes of the samples were studied by SEM. The dielectric and electric properties of the synthesized composites were measured using impedance spectroscopy as a function of frequency and as a function of temperature.

3. Results and discussion

3.1. X-ray diffraction analysis

The XRD patterns of the different solid solutions (1-x) MT – x BZT that were calcined at 1000 °C/4h are collected in the 2θ angle range of 5° − 80°, and presented in Fig. 2. It is evident that the pure MT (x = 0.0) crystallizes in the hexagonal perovskite structure without any additional peaks (Jo et al., 2015). The XRD patterns of the pure BZT sample (x = 1.0) indicate that all the peaks have been indexed, and correspond to the tetragonal phase without the presence of secondary peaks (Elbasset et al., 2015), while the XRD results of the solid solutions (1-x) MT – x BZT with $0.9 \geq x \geq 0.1$, show the coexistence of the hexagonal and the tetragonal phases. The structure of BZT-MT composite ceramics gradually transitions from the hexagonal phase to the tetragonal phase as the BZT concentration increases. This evolution shows that the Ba^{2+}, Zr^{2+}, and Ti^{4+} ions are completely diffused into the host lattice of the MT structures to form a solid solution.

To analyze the structural change, crystal system, and lattice parameters variation of (1-x) MT – x BZT composite samples, Rietveld refinement was performed utilizing the Fullprof software. The refinement quality is related to the reliability factor χ^2 which represents the ratio between the experimental and calculated patterns and indicates the good crystallinity of the powder ($\chi^2 < 2$ indicate a higher crystallinity of the powder). The refinement results are presented in Fig. 3.

For pure MT powder, it was adjusted with a hexagonal phase of R-3 space group. As depicted in Fig. 3.a, the refinement was successful and the fitted unit cell parameters are a = b = 5.0529 Å, c = 13.897 Å, α = β = γ = 90°, V = 307.3712 Å with a $\chi^2 = 0.949$. These results are in a good agreement with those reported by the researchers in the literature (Elbasset et al., 2015). For pure BZT sample, the spectrum fitting was performed with the tetragonal phase of P4mm space group, the refinement determined the following lattice parameters a = b = 4.0181 Å, c = 4.0168 Å, α = β = 90°, γ = 120°, V = 65.1977 Å with a χ^2=0.96. The obtained results are in accord with that reported in the previously studies (Jo et al., 2015). Furthermore, (1-x) MT – x BZT composites with × ranging from 0.1 to 0.9, the fitting of the solid solution was executed considering a two-phase system, and a considerable χ2 values were obtained between 0.90 and 1.66. Therefore, we can conclude that the calculated models and the measured models are in a good agreement, indicating the reliability of the refinement process and the high crystallinity of the prepared samples.

The obtained parameters corresponding to different compositions are grouped in Table 1. the unit cell parameters (a) and (c) evolve with high composition of BZT concentration, indicating a gradual transition from the hexagonal phase to the tetragonal phase. Moreover, the tetragonality (c/a) of BZT reduces largely as the BZT content rises, suggesting the tendency to the cubic phase. The variation of lattice parameters in zigzag could be attributed to cation substitution, the Mg^{2+} (ionic radius = 0.072 nm, coordination number = 6) ions can substitute Ti^{4+} (0.061 nm, CN = 6), or Ba^{2+} (*CN* = 12), or Zr^{4+} (0.072 nm, CN = 6) sites.

3.2. Rietveld refinement

(See).

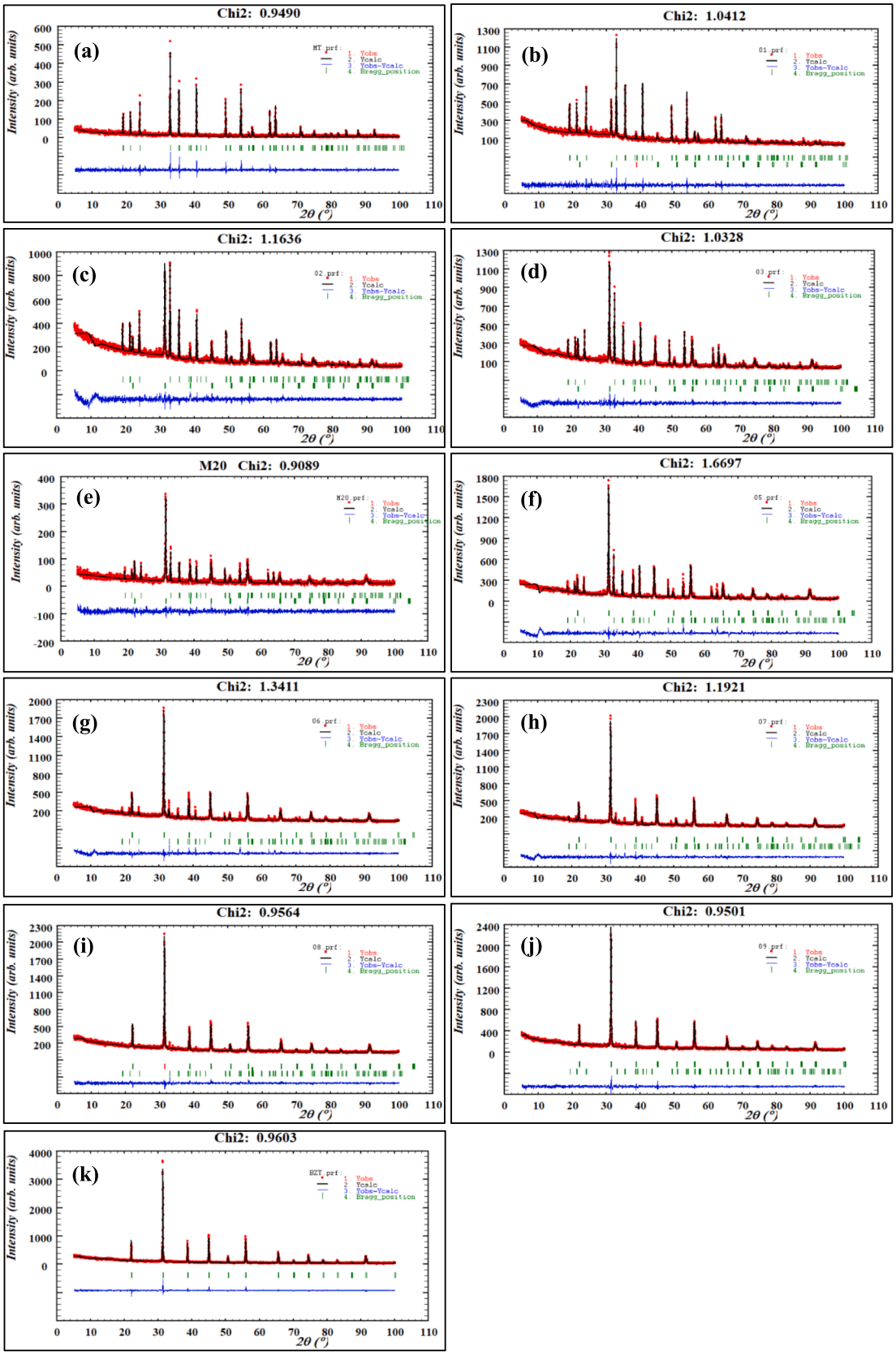

Fig. 3. Rietveld refinement of (1-x) MT – x BZT composites for x = 0.0 (a), 0.1 (b), 0.2 (c), 0.3 (d), 0.4 (e), 0.5 (f), 0.6 (g), 0.7 (h), 0.8 (i), 0.9 (j), 1.0 (k).

Table 1
Parameters of (1-x) MT – x BZT obtained via the Rietveld refinement.

x	x BZT			(1-x) MT		V	χ2
	Tetragonal (P4mm)			Hexagonal (R −3)			
	a = b (A°)	c (A°)	c/a	a = b (A°)	c (A°)		
0.0	….	….	….	5.0533	13.8990	307.3712	0.949
0.1	3.9913	4.0328	1.010397	5.0526	13.8986	307.2808	1.04
0.2	4.0191	4.0422	1.005747	5.0548	13.9067	307.7250	1.16
0.3	4.0221	4.0303	1.002038	5.0520	13.8963	307.1534	1.03
0.4	4.0284	4.0203	0.997989	5.0531	13.8978	307.3273	0.90
0.5	4.0220	4.0317	1.002411	5.0527	13.8965	307.2409	1.66
0.6	4.0237	4.0320	1.002062	5.0535	13.9020	307.4634	1.34
0.7	4.0237	4.0329	1.002286	5.0517	13.8955	307.0993	1.19
0.8	4.0249	4.0315	1.001639	5.0539	13.9016	307.5081	0.95
0.9	4.0232	4.0330	1.002435	5.0531	13.8977	307.3125	0.95
1.0	4.0250	4.0243	0.999676	…..	…..	65.1977	0.96

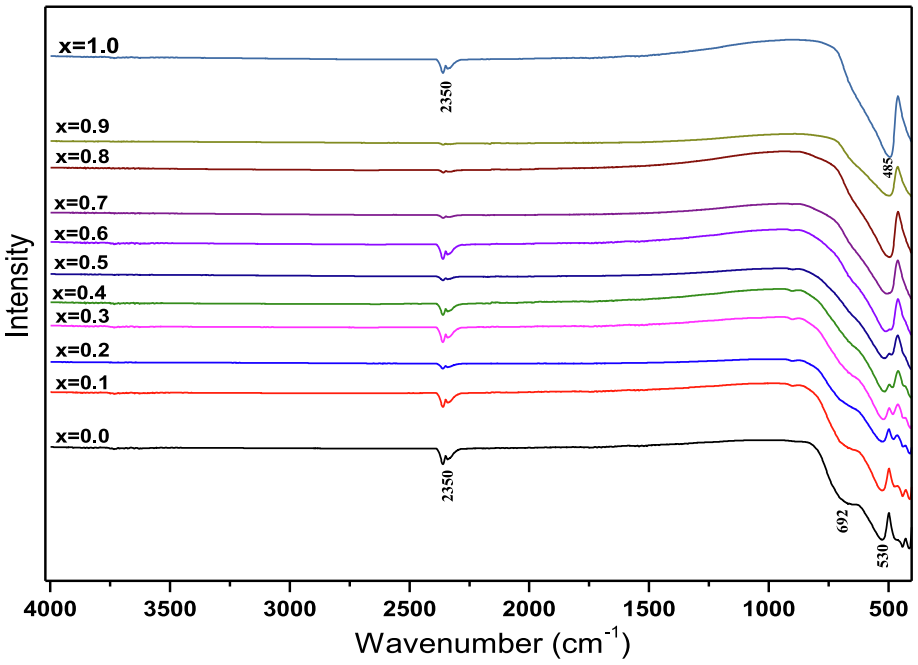

Fig. 4. FT-IR spectra of (1-x) MT – x BZT composites measured at room temperature.

3.3. Fourier-transform infrared spectroscopy analysis

To understand the crystal structure, we conducted the Fourier-transform infrared spectroscopy (FT-IR). This technique uses the vibrations of molecules, more specifically, the variations of these vibrations that occur when the sample is exposed to an electromagnetic wave of adequate frequency. Fig. 4 represent the FT-IR spectra of (1-x) MT – x BZT powders for different × percentage (x = 0.0 – 1.0) in wavenumber range of 450–4000 cm^{-1}. The FT-IR data shows two different absorption areas, that change with the BZT content. The first area with a large band and it's located at a wavenumber range of 720–450 cm^{-1}, and for the second area is found at a high wavenumber range of 2350 cm^{-1}. However, the first absorption area reveals the MT's characteristic bands at 530 and 692 cm^{-1}. These bands are assigned to the stretching vibration of M−O bonds (Ti-O and Mg-O), confirming the hexagonal structure (space group R-3) of the sample. The obtained results are in good accordance with those reported by H. Yang et *al.* for $MgTiO_3$ ceramic (Yang et al., 2020), and by R. Bahloul et *al.* for the $CdTiO_3$ ceramic (Bahloul et al., 2017). As the BZT concentration increases in the MT lattice, the characteristic bands of M−O shift to the lower energy values from 530 cm^{-1} in pure MT to 485 cm^{-1} in pure BZT, indicating the change in the unit cell size. The second absorption area attributed to symmetrical and antisymmetric vibrations (stretching of carboxyl groups (COO^{-})) in the prepared samples. The obtained FT-IR results are in good accord with those of XRD and Rietveld refinement.

3.4. SEM analysis

Microstructural analysis is an important tool for evaluating the size and shape of the grains, as well as the porosity, which considerably affects the dielectric properties of the material. For that reason, the morphology surface of the prepared ceramics was examined using SEM. The SEM micrographs of the (1-x) MT – x BZT composites, sintered at 1100 °C/8h, at a scale of 1 μm are presented in Fig. 5. For the pure MT (Fig. 5. a), the obtained grains are homogeneous in size, exhibiting a relatively regular and quasi-quadratic shape, with an average particle size around 1260.75 nm. The achieved results are similar to those reported by V. Sharon Samyuktha et *al.* in their study of the surface morphology and microstructure of $MgTiO_3$ (Sharon Samyuktha et al., 2016). It is well observed that the size and shape of the samples change depending on the BZT content. Fig. 5 shows that the grains shape becomes more semi-spherical with a high number of pores and a less homogeneity and grain size with a big concentration of BZT (Table 2). This evolution can be explained by the coexistence of the tetragonal and

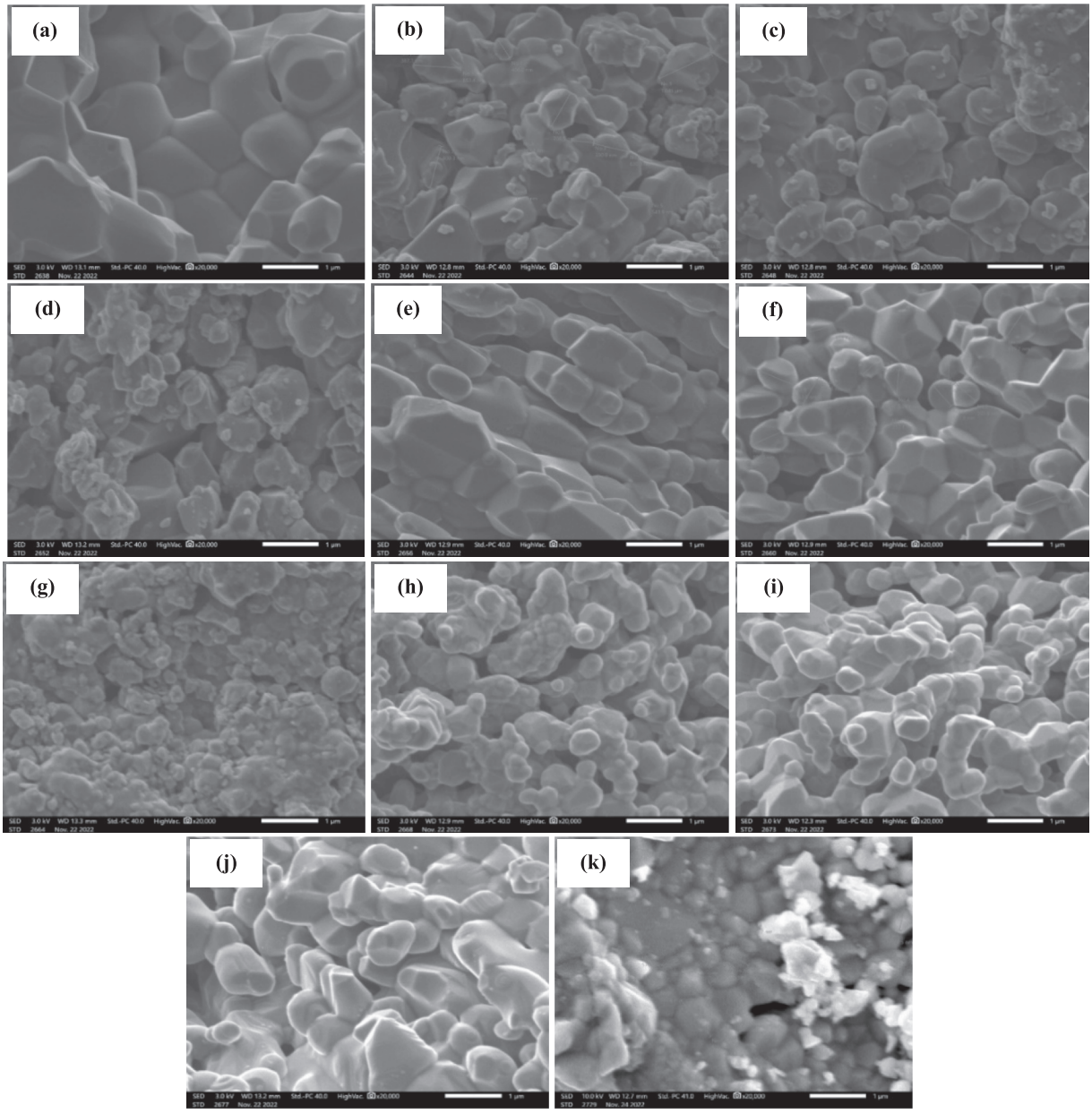

Fig. 5. SEM micrographs of (1-x) MT – x BZT samples for x = 0.0 (a), 0.1 (b), 0.2 (c), 0.3 (d), 0.4 (e), 0.5 (f), 0.6 (g), 0.7 (h), 0.8 (i), 0.9 (j), 1.0 (k).

Table 2
Average grains size of (1-x) MT – x BZT solid solution composition.

x	Average grains size (nm)
0.0	1260.75
0.1	1076.97
0.2	903.025
0.3	701.225
0.4	667.1
0.5	596.225
0.6	344.27
0.7	434.87
0.8	474.17
0.9	489.57
1.0	360.67

hexagonal phases, as it indicated previously in the XRD results. A similar change in the shape and the size of the grains were observed in the previous studies, such as the study reported by L.N. Gao et *al.* on the $BaZr_{0.2}Ti_{0.8}O_3$ – $MgTiO_3$ ceramics (Gao et al., 2008), and the work reported by R. Pengrong et *al.* for the (1-x) $BaZr_{0.25}Ti_{0.75}O_3$ – x MgO samples (Ren et al., 2011). Furthermore, a significant decrease in grains size is observed for the sample with x = 0.6, indicating that the grains size is minimal with a good density (Fig. 5. g). For the pure BZT sample (Fig. 5.k), the majority of the grains are homogeneous with a semi-spherical shape. This observation is in a good accord with Wei Cai et al. (Cai et al., 2009).

3.5. *Dielectric properties*

The variation of dielectric permittivity $(\varepsilon_r^{'})$ as a function of frequency (100 Hz – 2 MHz) of (1-x) MT – x BZT composites at different temperatures (Tam – 500 °C) is presented in Fig. 6. It clearly shows that for × between 0.0 and 0.6, the $\varepsilon_r^{'}$ decreases rapidly at low frequency regions,

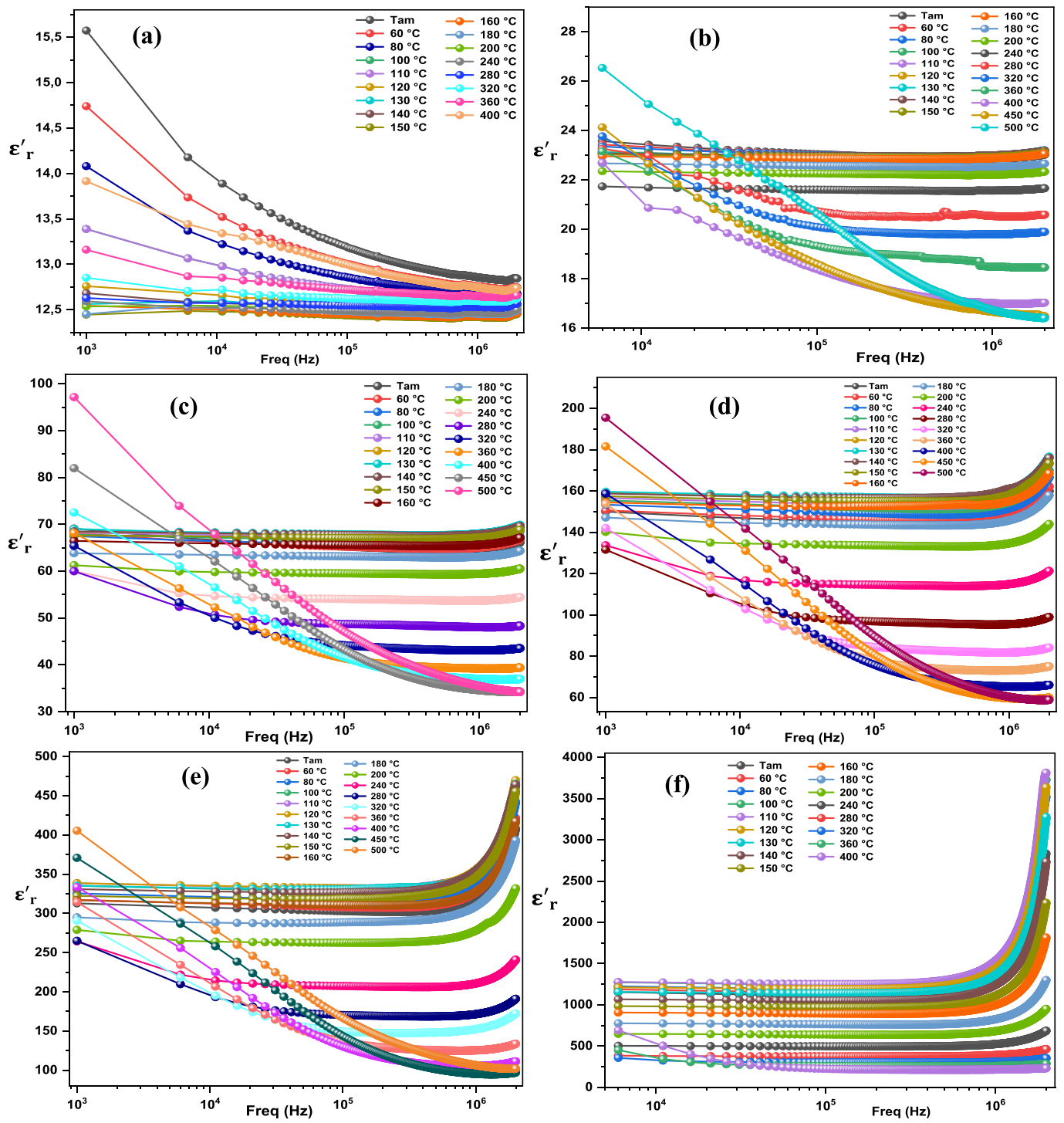

Fig. 6. Variation of the dielectric permittivity as a function of frequency for (1 – x) MT – x BZT composites with x = 0.0 (a), 0.2 (b), 0.4 (c), 0.6 (d), 0.8 (e), 1.0 (f).

then it remains constant and independent of frequency at high ranges. The high $\varepsilon_r^{'}$ values were observed in the low frequencies, it is caused by the polarization of space charge, which relates to the accumulation of free charges at the grain boundary and at the interface of the electrode and the sample. This effect is also owed to the oscillation of the induced dipoles following the applied external electric field. Furthermore, as the frequency increases, the dipoles start not following the applied electric field anymore, and that explains the observed reduction in $\varepsilon_r^{'}$ value at higher frequencies. In a similar study, N. Gouitaa et *al.* investigated (1-x) $CaTiO_3$–x$FeTiO_3$ composites with various compositions (x = 0.0 to 1.0) and observed the same behavior in their research (Gouitaa et al., 2022). However, for the percentage of BZT above 0.6, two different regions can be distinguished. The first one in the low frequency range where $\varepsilon_r^{'}$ remains constant forming a plateau behavior, followed by a second one at high frequency range with high dispersion. The observed dispersion could be attributed to the polarization mechanism associated with the thermoactivated conduction of mobile ions and/or other defects within the material.

Fig. 7. shows the variation of the $\varepsilon_r^{'}$ at different frequencies as a function of temperature, ranging from ambient temperature to 500 °C,

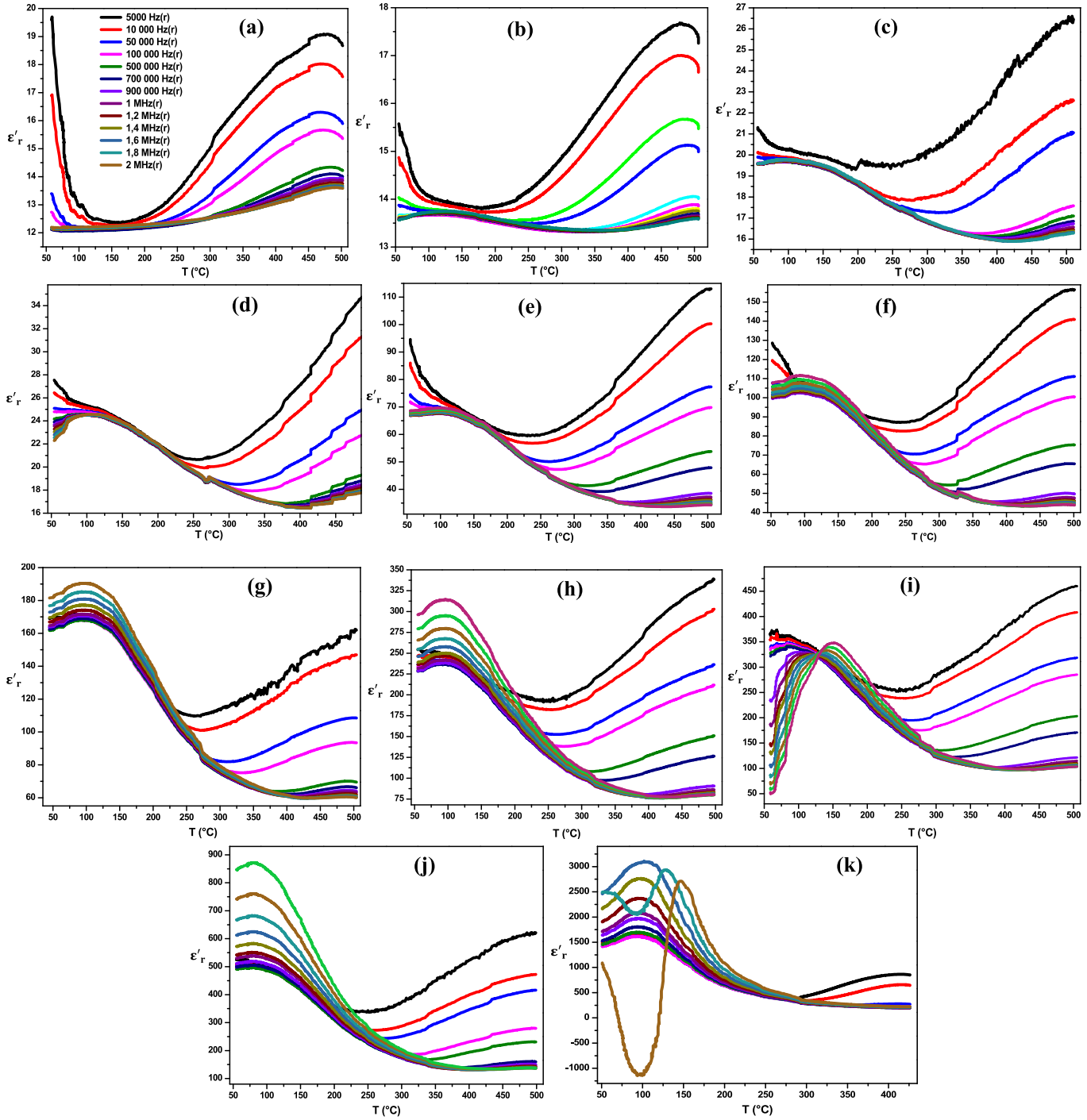

Fig. 7. Dielectric permittivity evolution as a function of temperature of (1 - x) MT - x BZT composites for x = 0.0 (a), 0.1 (b), 0.2 (c), 0.3 (d), 0.4 (e), 0.5 (f), 0.6 (g), 0.7 (h), 0.8 (i), 0.9 (j), 1.0 (k).

for various compositions of (1-x) MT – x BZT solid solution. We can notice that the pure MT compound (Fig. 7.a) exhibits an $\varepsilon_r^{'}$ value of 17 at ambient temperature, which is well suited to the literature (Ni et al., 2021; Shanker et al., 2012). Starting from 10 % of the BZT content, the (1-x) MT – x BZT composites reach a phase transition T_c from the ferroelectric phase (tetragonal symmetry) to the paraelectric phase (cubic symmetry). This transition has a diffuse character at low temperatures around 150 °C, corresponding to the BZT phase transition. Furthermore, the augmentation of $\varepsilon_r^{'}$ values is related to the high percentage of BZT, while the T_c shifts to lower temperatures for × values above 0.5. As mentioned in the SEM results, the BZT doping inhibits the grain growth at these percentages, increasing the internal stress inside the hetero-structured that is responsible for the downward shifting of T_c. This observation agrees with the results of Chen et *al.* (Chen et al., 2005).

The maximum value of $\varepsilon_r^{'}$ is relatively broad without any significant shift as a function of frequency, except for x = 0.8 which demonstrates a diffuse and non-relaxer behavior of the phase transition. For this percentage of BZT, we notice a clear deviation of this maximum at the higher temperatures as the frequency increases, suggesting a relaxer behavior of phase transition (Gouitaa et al., 2021). However, the relaxer behavior becomes more pronounced with a reduction in grain size, which is confirmed in this investigation. The parameters associated to

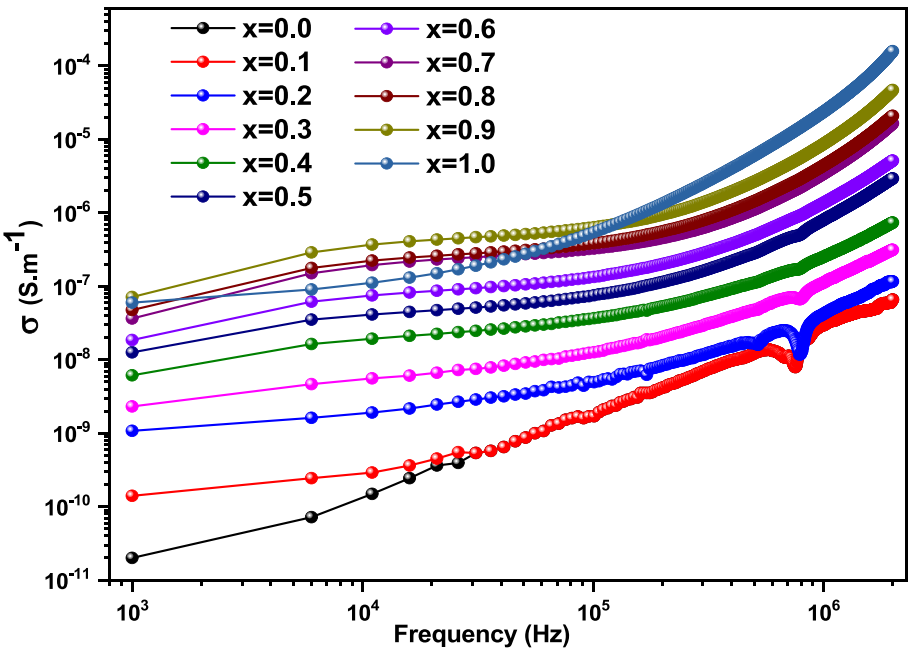

Fig. 8. Variation of conductivity as a function of frequency for (1-x) MT - x BZT (x = 0.0—1.0) ceramics at 240 °C.

Table 3
σ_{ac} values of (1-x) MT - x BZT composites at 2 MHz.

x content	0.0	0.1	0.2	0.3	0.4	0.5	0.6	0.7	0.8	0.9	1.0
σ_{ac} (S. m^{-1})	6.60×10^{-8}	8.03×10^{-8}	1.16×10^{-7}	3.14×10^{-7}	7.39×10^{-7}	2.94×10^{-6}	5.15×10^{-6}	1.65×10^{-5}	2.09×10^{-5}	4.70×10^{-5}	1.59×10^{-4}

these relaxer and diffuse behaviors, as found in this work, will be studied in the next works. By comparing these results with those reported in the literature by L.N. Gao et *al.* (Gao et al., 2008), the broad phase transition observed in the present study has not been reported for BZT-MT composites, possibly because the Zr content in BZT chosen in their study at 0.2 (20 %), which is higher than the percentage chosen in the current study.

For pure BZT material (Fig. 7.k), the $\varepsilon_r^{'}$ reaches maximum values about 3150 at room temperature, which is more higher than that mentioned by A. El basset et *al.*, who studied the effect of the Zr rate on

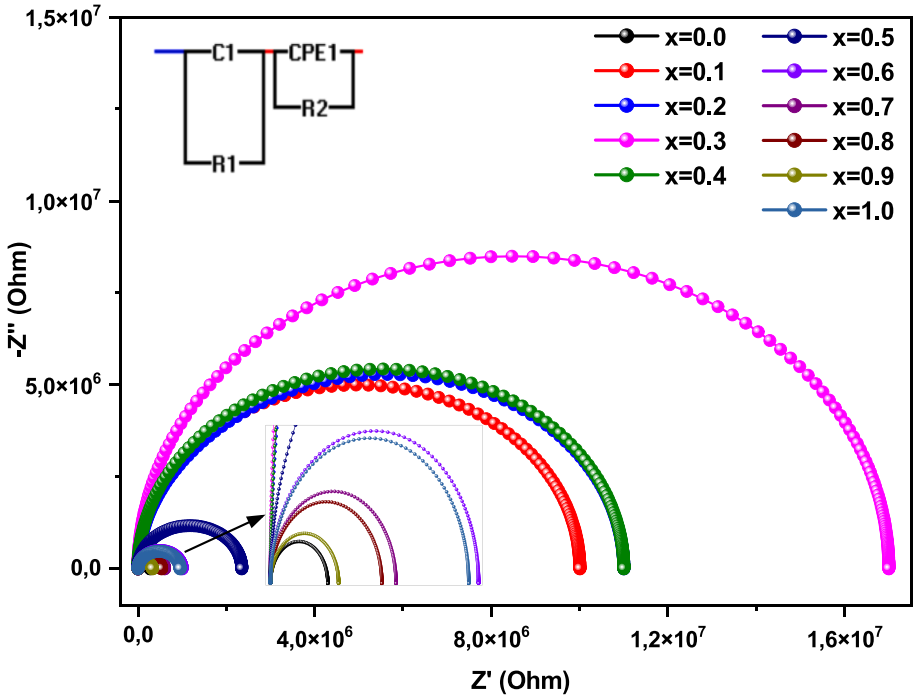

Fig. 9. Cole-Cole plots of the (1-x) MT - x BZT (x = 0—100 %) ceramics at 240 °C.

the structural and dielectric properties of BTZ_x samples ($0 \leq x \leq 15$ %) by the sol–gel process ($\varepsilon'_{r,max} = 2830$) (Elbasset et al., 2015).

3.6. Electric properties

Fig. 8 depicts the evolution of conductivity (σ) as a function of frequency (10 Hz – 2 MHz) at 240 °C of tested temperature of the (1 – x) MT – x BZT samples with different compositions (x = 0.0—1.0). The σ plots can be remarkably divided into two different regions. In the first region at low frequencies, the σ remains relatively constant, indicating a linear behavior. This shows that it is independent of frequency, which can be assigned to the long-range migration of the charge carriers, confirming the direct current conductivity (DC conductivity σ_{dc}). Therefore, in this region the conductivity is followed by a continuous current. In the second region at high frequencies, the σ starts to increase as a function of frequency with a highly dispersive behavior. This behavior is caused by the successive hopping of charges over a long range (AC conductivity σ_{ac}) (Gouitaa et al., 2017). It's also clear that the addition of BZT enhanced σ (Table 3). Thus, the σ values of (1-x) MT - x BZT solid solutions increase with high concentrations of the BZT content. The obtained results are in good agreement with those of M. Slaoui et *al.*, who studied (1-x) CCTO - x PT samples for x = 0.0 to 1.0 (Slaoui et al., 2021).

The impedance characteristic was analyzed using the Cole-Cole function associated with the processes of grains, grains boundaries, and electrode. Fig. 9 presents the Cole-Cole tracing of (1-x) MT - x BZT ceramics with various compositions (x = 0.0 – 1.0) at a temperature of 240 °C. These plots can be fitted by a circuit composed of R-C (R-C in parallel) in series with an R-CPE (R-CPE in parallel). The fitted Cole-Cole curves obtained for all compositions are characterized by a tendency to curve to the real abscissa axis, creating semicircles with their centers located on a line below the real axis. This phenomenon demonstrates the presence of a non-Debye type of relaxation mechanism in this solution solid (Gouitaa et al., 2018). For the compositions range from x = 0.0 to x = 0.3, it can be observed that the semicircle radius decreases with high concentrations of BZT content, showing a low grain boundary resistivity (R_{GB}). However, the radius grows as the concentration of BZT rises at × > 0.3, indicating an enhancement of R_{GB}.

4. Conclusion

A series of (1-x) MT– x BZT (x = 0.0 – 1.0) composite ceramics were successfully synthesized through the sol–gel process. The XRD and Rietveld refinement studies showed that all the prepared compounds crystallize in the perovskite structure without the presence of any secondary phases, indicating that a calcination treatment at 1000 °C for 4 h is suitable for the complete crystallization of the samples. SEM micrographs showed a transformation in grain shape from semi-quadratic to semi-spherical, and a decrease in size with the increase of BZT content. Dielectric permittivity as a function of frequency and temperature confirms a phase transition from the ferroelectric phase to the paraelectric phase with a diffuse character. Thus, the dielectric permittivity values enhanced and T_c shifted to the lower temperatures as the BZT content increases. the electrical properties indicate that the conductivity evolved with higher BZT content. The Cole-Cole plots demonstrate that the grain boundary resistivity (R_{GB}) has the higher values for x > 0.3 and confirm the presence of a non-Debye relaxation mechanism.

These results provide valuable insights into the structural, microstructural, dielectric, and electrical properties of (1-x) MT– x BZT composite ceramics, approving that the synthesized ceramics are promising materials for the development of advanced applications in various technological fields.

Declaration of Competing Interest

The authors declare that they have no known competing financial interests or personal relationships that could have appeared to influence the work reported in this paper.

References

Amu-Darko, J.N.O., Zhang, C., Hussain, S., Otoo, S.L., Agyemang, M.F., 2022. Relaxor ferroelectric and dielectric properties of (1–x)Ba(Zr0.1Ti0.9)O3–xBa(Mg1/3Ta2/3)O3 ceramics. Trans. Nonferrous Met. Soc. China (English Ed.) 32 (4), 1242–1252. https://doi.org/10.1016/S1003-6326(22)65870-9.

Bahloul, R., Sayouri, S., Limame, K., Mustapha Yahyaoui, M., Jaber, B., Laanab, L., 2017. Temperature effect on the structural and the optical properties of sol gel $CdTiO_3$ nanopowders. J. Ceram. Process. Res. 18 (4), 329–335.

Baryshnikov, S.V., Charnaya, E.V., Milinskii, A.Y., Antonov, A.A., Bugaev, A.S., 2015. Phase transitions in the (BaTiO3)x/(BiFeO3)1–x composite ceramics: Dielectric studies. Compos. B Eng. 80, 15–19. https://doi.org/10.1016/j.compositesb.2015.05.037.

Binhayeeniyi, N., Sukvisut, P., Thanachayanont, C., Muensit, S., 2010. Physical and electromechanical properties of barium zirconium titanate synthesized at low-sintering temperature. Mater. Lett. 64 (3), 305–308. https://doi.org/10.1016/j.matlet.2009.10.069.

Cai, W., Fu, C., Gao, J., Chen, X., Zhang, Q., 2009. Microstructure and dielectric properties of barium zirconate titanate ceramics by two methods. Integr. Ferroelectr. 113 (1), 83–94. https://doi.org/10.1080/10584581003785393.

Chen, Z., et al., 2020. Achieving high-energy storage performance in $0.67Bi_{1-x}Sm_xFeO_3$-$0.33BaTiO_3$ lead-free relaxor ferroelectric ceramics. Ceram. Int. 46 (8), 11549–11555. https://doi.org/10.1016/j.ceramint.2020.01.181.

Ying Chen, Xian-Lin Dong, Rui-Hong Liang, Jian-Tong Li, Yong-Ling Wang, "Dielectric properties of $Ba_{0.6}Sr_{0.4}TiO_3$ / Mg_2SiO_4/MgO composite ceramics. *Journal of Applied Physics,* 15 September 2005; 98 (6): 064107–064111. 10.1063/1.2058194.

Dai, Z., et al., 2020. Effective strategy to achieve excellent energy storage properties in lead-free $BaTiO_3$-based bulk ceramics. ACS Appl. Mater. Interfaces 12 (27), 30289–30296. https://doi.org/10.1021/acsami.0c02832.

A. Elbasset *et al.*, "Influence of Zr on structure and dielectric behavior of $BaTiO_3$ ceramics," *Indian J. Sci. Technol.*, vol. 8, no. 13, 2015, doi: 10.17485/ijst/2015/v8i13/56574.

M. Fahad, R. Thangavel, and P. M. Sarun, "Scaling behavior of the $BaZr_{0.1}Ti_{0.9}O_3$ (BZT) dielectric ceramic at the elevated temperatures (400 °C – 540 °C)," *Mater. Sci. Eng. B Solid-State Mater. Adv. Technol.*, vol. 283, no. December, 2022, doi: 10.1016/j.mseb.2022.115837.

Gao, L.N., Zhai, J.W., Yao, X., Xu, Z.K., 2008. Dielectric properties of heterostructured BZT thin films prepared by sol-gel technique. Mater. Lett. 62 (17–18), 3198–3200. https://doi.org/10.1016/j.matlet.2008.02.018.

Gouitaa, N., Lamcharfi, T., Bouayad, M., Abdi, F., Hadi, N., 2018. Impedance, modulus and conductivity studies of Fe3+ doped BaTiO3 ceramics prepared by solid state method. J. Mater. Sci.: Mater. Electron. 29 (8), 6797–6804. https://doi.org/10.1007/s10854-018-8666-3.

Gouitaa, N., Lamcharfi, T., Abdi, F., Echatoui, N.S., Amarass, M., 2021. " Diffuse and relaxor phase transitions of Ba0.95Bi0.05Ti1-xFexO3 ceramics at x=0.00 to 1.00 of Fe content, prepared by solid state method". *IOP Conf. Ser. Mater.* Sci. Eng. 1160 (1), 012006 https://doi.org/10.1088/1757-899x/1160/1/012006.

Gouitaa, N., Ahjyaje, F.Z., Lamcharfi, T., Abdi, F., Haddad, M., 2022. High dielectric permittivity and low transition temperature of (1–x)CaTiO3 –xFeTiO3 inorganic composites (x = 0.0 to 1.0). Russ. J. Inorg. Chem. 67 (11), 1868–1879. https://doi.org/10.1134/S0036023622100588.

N. Gouitaa, T. Lamcharfi, Mf. Bouayad, F. Abdi, N.S. Echatoui and N. Hadi. " Dielectric anomalies of $BaTi_{1-x}Fe_xO_3$ ceramics for x = 0.0 to 0.6 of Fe doping concentration, " *Asian Journal of Chemistry*, vol. 29, no. 10 (2017) 2143-2148. 10.14233/ajchem.2017.20653.

Hu, Q., et al., 2020. Achieve ultrahigh energy storage performance in BaTiO3–Bi(Mg1/2Ti1/2)O3 relaxor ferroelectric ceramics via nano-scale polarization mismatch and reconstruction. Nano Energy 67, 104264. https://doi.org/10.1016/j.nanoen.2019.104264.

Jamil, N.H.J., Izzuddin, I., Zainuddin, Z., Jumali, M.H.H., 2015. Microstructural studies of nanocrystalline barium zirconium titanate (BZT) for piezoelectric applications. AIP Conf. Proc. 1678 https://doi.org/10.1063/1.4931265.

Jo, H.J., Kim, J.S., Kim, E.S., 2015. Microwave dielectric properties of $MgTiO_3$-based ceramics. Ceram. Int. 41 (S1), S530–S536. https://doi.org/10.1016/j.ceramint.2015.03.142.

Kumar, T.S., Kumar, A., James, A.R., Pamu, D., 2012. Enhanced microwave dielectric properties of $MgTiO_3$ ceramics prepared by mechanochemical method. J. Aust. Ceram. Soc. 48 (1), 96–101.

B. Li *et al.*, "Structure and microwave dielectric properties of $(Zn_{1/3}Nb_{2/3})^{4+}$ co-substituted $MgTiO_3$ ceramic," *Mater. Sci. Eng. B Solid-State Mater. Adv. Technol.*, vol. 276, no. December 2021, p. 115572, 2022, doi: 10.1016/j.mseb.2021.115572.

Mondal, T., Das, S., Sinha, T.P., Sarun, P.M., 2018. Dielectric relaxation and study of electrical conduction mechanism in $BaZr_{0.1}Ti_{0.9}O_3$ ceramics by correlated barrier hopping model. Mater. Sci. Pol. 36 (1), 112–122. https://doi.org/10.1515/msp-2018-0013.

Ni, Y., Liu, K., Wang, J., Sun, H., Du, Y., Liu, W., 2021. Establishment of constitutive models and numerical simulation of dry pressing and solid state sintering processes of $MgTiO_3$ ceramic. Ceram. Int. 47 (7), 8769–8780. https://doi.org/10.1016/j.ceramint.2020.11.242.

Ren, P., Fan, H., Wang, X., Tan, X., 2011. Modified tunable dielectric properties by addition of MgO on $BaZr_{0.25}Ti_{0.75}O_3$ ceramics. Mater. Res. Bull. 46 (12), 2308–2311. https://doi.org/10.1016/j.materresbull.2011.08.054.

Sateesh, P., Omprakash, J., Kumar, G.S., Prasad, G., 2015. Studies of phase transition and impedance behavior of Ba(Zr, Ti) O3 ceramics. J. Adv. Dielectr. 5 (1), 1–13. https://doi.org/10.1142/S2010135X15500022.

Shanker, V., Kumar, S., Surendar, T., 2012. Dielectric behaviour of sodium and potassium doped magnesium titanate. Bull. Mater. Sci. 35 (7), 1165–1171. https://doi.org/10.1007/s12034-012-0399-y.

Sharon Samyuktha, V., Prof, T., Rao, S., Prof, R., Suvarna, P., 2016. Synthesis and dielectric properties of $MgTiO_3$ ceramic material. Int. J. Eng. Res. V5 (05), 245–249. https://doi.org/10.17577/ijertv5is050349.

Shukla, J., Bisen, S., Khan, M., Mishra, A., 2019. Study of structural and optical properties of barium zirconate titanate prepared through sol - Gel auto combustion method. AIP Conf. Proc. 2115 (July), 1–5. https://doi.org/10.1063/1.5113033.

Slaoui, M., Gouitaa, N., Lahrichi, A., Harrach, A., Haddad, M., Lamcharfi, T., 2021. Synthesis and physico-chemical characterization of solid solution (1–x)CCTO-xPbTiO3. Asian J. Chem. 33 (6), 1208–1214. https://doi.org/10.14233/ajchem.2021.23134.

Wang, M., Yan, D., 2021. Improved crystalline structure and sintering characteristics of nonstoichiometric $MgTiO_3$ ceramics by sol–gel method. J. Sol-Gel Sci. Technol. 97 (2), 365–372. https://doi.org/10.1007/s10971-020-05458-x.

Xu, P., et al., 2018. Influence of $MgTiO_3$-doping on microstructure and dielectric properties of $CaCu_3Ti_4O_{12}$ ceramics. J. Electron. Mater. 47 (9), 5582–5587. https://doi.org/10.1007/s11664-018-6450-z.

Xu, Y., et al., 2019. Effect of MgO addition on sintering temperature, crystal structure, dielectric and ferroelectric properties of lead-free BZT ceramics. J. Mater. Sci. Mater. Electron. https://doi.org/10.1007/s10854-019-01073-x.

Yang, H., et al., 2020. Novel BaTiO3-based, Ag/Pd-compatible lead-free relaxors with superior energy storage performance. ACS Appl. Mater. Interfaces 12 (39), 43942–43949. https://doi.org/10.1021/acsami.0c13057.

Yang, Z., Du, H., Jin, L., Poelman, D., 2021. High-performance lead-free bulk ceramics for electrical energy storage applications: design strategies and challenges. J. Mater. Chem. A 9 (34), 18026–18085. https://doi.org/10.1039/d1ta04504k.

Zheng, K., et al., 2023. The Synthesis and Domain Structures of Single-Crystal-Like Mesoscale $BaTiO_3$ Plates. Crystals 13 (3), 1–10. https://doi.org/10.3390/cryst13030538.

Zhou, M., Liang, R., Zhou, Z., Dong, X., 2019. Combining high energy efficiency and fast charge-discharge capability in novel $BaTiO_3$-based relaxor ferroelectric ceramic for energy-storage. Ceram. Int. 45 (3), 3582–3590. https://doi.org/10.1016/j.ceramint.2018.11.018.